Applied Catalysis B: Environmental 144 (2014) 570–579

Contents lists available at ScienceDirect

Applied Catalysis B: Environmental

journal homepage: www.elsevier.com/locate/apcatb

# Ti-based layered double hydroxides: Efficient photocatalysts for azo dyes degradation under visible light

Sheng-Jie Xia, Feng-Xian Liu, Zhe-Ming Ni*, Wei Shi, Ji-Long Xue, Ping-Ping Qian

*College of Chemical Engineering and Materials Science, Zhejiang University of Technology, Hangzhou 310032, PR China*

ARTICLE INFO

*Article history:*
Received 1 May 2013
Received in revised form 22 July 2013
Accepted 28 July 2013
Available online 7 August 2013

*Keywords:*
Ti-based layered double hydroxides
Photocatalysis
Azo dyes
Kinetics
Degradation mechanism

ABSTRACT

Three types of Ti-based Layered Double Hydroxides (Zn/Ti–$NO_3$–LDHs with Ti element on LDH sheet, Zn/Al–Ti/Schiff–base–LDHs with Ti element in LDH interlayer and $CeO_2$/ZnTi–LDH composite containing $TiO_2$) were synthesized by different environmental friendly methods. Their activities of photocatalytic degradation of Methyl orange and Methylene blue under visible light were tested. Ti-based LDHs were characterized by XRD, FT-IR, BET and ICP-AES, confirming the formation of pure LDH phase with good crystal structure. The as-synthesized Ti-based LDH materials showed the narrow band gap (all smaller than 3.0 eV) and high removal efficiency for Methyl orange and Methylene blue under visible light, and the decomposition performance of these dyes decreased in the order of $CeO_2$/ZnTi–LDH composite > Zn/Al–Ti/Schiff–base–LDHs > Zn/Ti–$NO_3$–LDHs. In addition, the kinetics and possible mechanisms for photocatalytic degradation on Methyl orange and Methylene blue were also discussed in details. Moreover, the thermal regeneration for re-use of Zn/Al–Ti/SB–LDHs after photoreaction was feasible for at least three cycles (degradation amount still over 85%).



## 1. Introduction

Photo catalysis is the process, during which the nano semiconductive materials convert luminous energy into chemical energy and at the same time synthesize or decompose organic or inorganic compounds. This technique is based on the band theory and the n-type semiconductor is used as the photosensitized material, the semi-conductor material used in this process is mainly metal oxide or metal sulfide [1,2]. $TiO_2$ is one of the most widely used photo catalyst, based on its good properties like chemically inert, non-toxic to organisms, well-resourced, high energy gap, to create photoelectron and hole with high electric potential, strong oxidation and reduction, etc. But at the same time, as this material has the disadvantages like very low specific surface area, low surface adsorption rate, difficult to recycle, etc., the application of it in industry is constricted. Other major issues about this material include: (1) hard to process industrial disposal with high concentration of wastes because of its low quantum yield (4%); (2) $TiO_2$ could only absorb the ultraviolet part of the solar light, and therefore has low efficiency for conversion; (3) could not be loaded evenly and strongly on other supporting materials when maintaining high activity and other good chemical and physical properties, thus making the photocatalyst not easy to be reused [3–5]. Based on the above mentioned, developing recyclable semi-conductor material which has high quantum yield and visible light absorption rate is one of the major task for the photocatalysis area [6].

Layered double hydroxides (LDHs) are a class of host–guest layered solids with the general formula $[M_{1-x}^{2+}M_x^{3+}(OH)_2]^{x+}A_{x/n}^{n-} \cdot mH_2O$, where $M^{2+}$ and $M^{3+}$ are di- and trivalent metal cations, $A^{n-}$ denotes exchangeable organic or inorganic anion with negative charge $n$, $m$ is the number of interlayer water molecule and $x$ ($= M^{3+}/(M^{2+} + M^{3+})$) is the layer charge density of LDHs [7–9]. Recently, LDHs have drawn a lot of attention in the environmental waste treatment study for its properties like special layered structure, exchangeable of the anions, high anion exchange capacity, easy to be synthesized and low costs [10]. With the consideration that LDHs have two or three different metals and that the proportion among these metals could be controlled, LDHs can be envisioned as providing the opportunity of having "doped composites". Because, that doping or composition would result in a state of defect energy between the valence band and conduction band, which would provide a spring board for photon generated electrons ($e^-$). And this photon generated electrons can activate valence band electrons transmit to conduction band by visible light with lower energy, which would make the absorption edge move to visible light region. Thus, it would reduce materials' the band gap energy, and also improve the photo-catalytic property. Researchers have been paying attention to LDHs being a candidate used as photocatalysis material for its special micro-structure, adjustable forbidden band gap, and recyclable properties [11–14]. It is still a

* Corresponding author. Tel.: +86 0571 88320373.
*E-mail addresses:* jchx@zjut.edu.cn, nzm@zjut.edu.cn (Z.-M. Ni).

0926-3373/$ – see front matter © 2013 Elsevier B.V. All rights reserved.
http://dx.doi.org/10.1016/j.apcatb.2013.07.060

new area to use LDHs as the photo catalyst, even though it is much easier to be re-used and has higher light absorption range compared to the $TiO_2$, the photocatalysis efficiency is still very low [15,16]. In recent years, researchers have found that the doping of Ti into LDHs could enhance the catalytic ability a lot [17,18]. Also, after being calcined under high temperature, bimetallic oxide could be formed, the second metal could be high dispersed and doped into the LDH materials, the photocatalysis of these materials could be dramatically improved [19,20]. Therefore, we have been working to synthesize LDHs with different Ti orientations, and combining the advantages of both $TiO_2$ and LDHs, the new synthesized material may display excellent photocatalytic performance degradation for azo dyes.

In this work, we have synthesized different types of Ti-based LDH materials: Zn/Ti–$NO_3$–LDHs with Ti element on LDH sheet, Zn/Al–Ti/Schiff–base–LDHs with Ti element in LDH interlayer and $CeO_2$/ZnTi–LDH composite containing $TiO_2$, by three different methods, and studied their activity for visible light photocatalytic Methyl orange and Methylene blue degradation. All the LDH mterials have shown good crystal structure based on the results from XRD, FT-IR, BET and ICP-AES analysis. Moreover, the degradation rate, kinetic parameters (Langmuir–Hinshelwood model), and the regeneration of Ti-based LDH materials have also been investigated. In addition, the photocatalytic degradation mechanism and the possible intermediate products are also discussed.

## 2. Experimental

### 2.1. Materials

Methyl orange ($C_{14}H_{14}N_3SO_3Na$, abbreviated as MO here), Methylene blue ($C_{16}H_{18}ClN_3S{\cdot}3H_2O$, abbreviated as MB here) and other reagents were all analytical grade (AR) and were used without further purification. There into, MO or MB were purchased from Zhejiang Shanghai SSS Reagent Co. Ltd. (China), and their solutions were prepared by dissolving MO or MB in deionized water, respectively; sodium 4-aminobenzoate and salicylaldehyde from Aldrich; and other reagents were all from Zhejiang Xiaoshan Fine Chemical Co. Ltd. In addition, Deionized water was decarbonated by boiling and bubbling $N_2$ before employing in all synthesis steps.

### 2.2. Preparation of samples

#### 2.2.1. Synthesis of Zn/Ti–$NO_3$–LDHs by coprecipitation

A typical synthetic procedure is as follows: an aqueous solution (80 mL) containing urea (26.0 g, 0.42 mol) was added dropwise to a solution (80 mL) containing 2 ml (0.008 mol) of $TiCl_4$ solution (the $TiCl_4$ solution was prepared by mixing $TiCl_4$ and HCl with the volume ratio as 1:1 at ice water bath) and 11.87 g (0.04 mol) of $Zn(NO_3)_2{\cdot}6H_2O$ (the molar ratio of $Zn^{2+}/Ti^{4+}$ is 5:1) with vigorous stirring at 40 °C until the final pH 9. Then, the produced suspension was stirred for 48 h at a refluxing temperature of 105 °C. The product was centrifuged and washed twice with deionized water and then once with anhydrous ethanol until the pH 7. Finally the sample was dried in vacuo at 65 °C for 24 h, then ground, giving the product Zn/Ti–$NO_3$–LDHs.

#### 2.2.2. Synthesis of Zn/Al–Ti/Schiff–base–LDHs by ion-exchange

*2.2.2.1. Preparation of Zn/Al–LDHs.* An aqueous solution (100 mL) containing NaOH (16.0 g, 0.4 mol) was added dropwise to a solution (150 mL) containing $Zn(NO_3)_2{\cdot}6H_2O$ (44.6 g, 0.15 mol) and $Al(NO_3)_3{\cdot}9H_2O$ (18.8 g, 0.05 mol) (initial Zn/Al = 3.0) with vigorous stirring until getting to the final pH 8.5. The resultant slurry was aged at 65 °C for 24 h, and then centrifuged and washed with deionized water until the pH 7, finally it was dried in vacuo at 85 °C for 18 h, then grounded, giving the product Zn/Al–$NO_3$–LDHs (the content of H, N and Zn, Al: H = 2.40%, N = 3.86%, Zn = 41.47%, Al = 6.05%).

*2.2.2.2. Preparation of Ti/Schiff–base.* In 250 ml flask, 100 ml of ethanol solution containing 6.12 g (50 mmol) salicylaldehyde was added dropwise into a solution containing 6.86 g (50 mmol) of sodium 4-aminobenzoate and 50 ml of ethanol with vigorous stirring for 30 min. Then, the reaction system was continuously stirred for 3 h at a refluxing temperature of 85 °C. The resultant slurry was then condensed, refrigerated, filtered, washed with ice-cold ethanol and dissolved with warm ethanol, after repeating the above-mentioned steps three times, finally the product was dried in vacuo oven at 60 °C for 6 h, giving the Schiff–base ligand ($C_{14}H_{10}NO_3Na$, 263 g/mol, abbreviated as SB, the yield = 62.5%, the content of C, H and N: C = 62.43%, H = 3.57%, N = 5.49%).

An ethanolic solution (60 mL) containing as-synthesized Schiff base ligand (0.711 g, 2.7 mmol) was added dropwise to a solution containing 0.17 ml (1.5 mmol) of $TiCl_4$ and 10 ml of ethanol with vigorous stirring under the $N_2$ atmosphere. Then, the produced suspension was continued stirred for 2 h at a refluxing temperature of 80 °C. The slurry was filtered, washed thrice with ethanol and recrystalized from diethyl ether, finally it was dried in vacuo oven at 65 °C for 6 h, giving the product Ti/Schiff–base complex $(C_{14}H_{10}NO_3Na)_2Ti$, 573.9 g/mol, abbreviated as Ti/SB, the yield = 78.3.%, the content of C, H, N and Ti: C = 58.17%, H = 3.46%, N = 4.85%, Ti = 8.85%).

*2.2.2.3. Preparation of Zn/Al–Ti/Schiff–base–LDHs.* The synthetic procedure of Zn/Al–Ti/Schiff–base–LDHs was the same like the ion-exchange method which is as follows: firstly, 50 ml of ethanol was added to 1.5 g dried Zn/Al–LDHs and stirred for 1 h; secondly, 0.75 mmol (0.429 g) of Ti/Schiff–base complex was transferred into the above mentioned ethanolic suspension of LDH, and the reaction system was refluxed at 80 °C for 24 h with constant stirring; finally, the product was isolated by filtration, washed with ethanol and kept overnight in vacuum at 65 °C, giving the product Zn/Al–Ti/Schiff–base–LDHs (abbreviated as Zn/Al–Ti/SB–LDHs, the content of C, H, N and Zn, Al, Ti: C = 16.64%, H = 1.51%, N = 2.68%, Zn = 27.87%, Al = 3.86%, Ti = 2.80%). The complete preparation pathway for the Ti/Schiff–base intercalated LDH material is depicted in Scheme 1.

#### 2.2.3. Synthesis of $CeO_2$/ZnTi–LDH composite by calcination

A typical synthetic procedure like the wet impregnation method is as follows: first, the Zn/Ti–LDH (10 g) was calcined at 500 °C for 6 h, taken out of the oven at this temperature, and immediately placed in a reactor in which a cerium nitrate solution was previously prepared (4.34 g $Ce(NO_3)_3{\cdot}6H_2O$ in 100 mL decarbonated water). Then, the product suspension was stirred and refluxed for 18 h at temperature of 85 °C. After impregnation, the mixtures were treated with 2 mol/L NaOH solution in order to generate the cerium oxide xerogel [21]. The as-prepared solid was filtered and washed with deionized water (30 mL × 2) and anhydrous ethanol (30 mL) until pH 7. Finally the sample was dried in vacuo at 65 °C for 18 h and calcined in the oven at 500 °C for 5 h, then ground, giving the product $CeO_2$/ZnTi–LDH composite.

### 2.3. Characterizations

Powder X-ray diffraction (XRD) patterns were recorded on a Rigaku RINT 2000 powder diffractometer, using Cu Kα radiation (λ = 1.54 Å) at 40 kV and 178 mA and scanning rate of 5°/min in the range of 5–70°.

Fourier transform infrared spectra (FT-IR) was obtained on a Bruker Vector 22 spectrophotometer in the range of

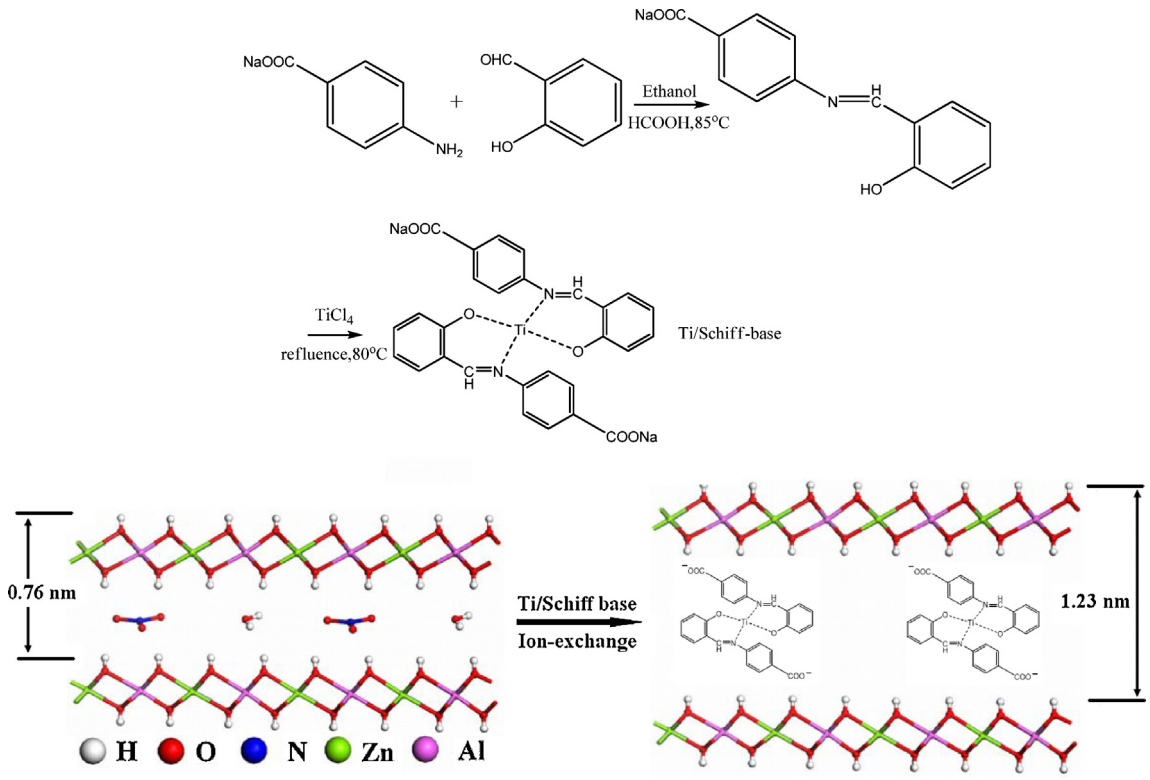


**Scheme 1.** The preparation pathway for the Zn/Al–Ti/Schiff–base–LDHs.

4000–400 $cm^{-1}$ with 2 $cm^{-1}$ resolution by using the standard KBr disk method (sample/KBr = 1/100).

Zn, Al, Ti and Ce element analysis were conducted using inductively coupled plasma atomic emission spectrometry (ICP-AES) on a IRIS Intrepid II XSP instrument. CHN, etc. elemental microanalyses were obtained on a ThermoFinnigan Italia S.P.A. elemental analyzer.

The pore structure of the Ti-based LDH materials was analyzed by $N_2$ adsorption–desorption at 77 K on a Micromeritics Instrument Corporation ASAP2020 M apparatus. Prior to the analysis, the samples were degassed in a vacuum at 120 °C for 6 h. The specific surface areas were calculated by the Brunauer–Emmett–Teller (BET) method, and the pore size distribution and total pore volume were determined by the Brunauer–Joyner–Hallenda (BJH) method using a Micromeritics Instrument Corporation Tristar II 3020 Analyzer.

Solid-state UV–vis diffuse reflectance spectra was recorded at room temperature in air by means of a Shimadzu UV-2550 spectrometer equipped with an integrating sphere attachment using $BaSO_4$ as background.

### 2.4. Photocatalytic reactions

The photo-catalytic activity of Ti-based LDHs was monitored by degradation of MO or MB under irradiation with visible light using a 350 W xenon lamp equipped with a constant temperature circulator with the temperature of 15 °C. Typically, a mixture of 50 mL of MO or MB (50 mg/L) solution and 50 mg of catalyst was vigorously stirred for 30 min to establish an adsorption/desorption equilibrium in dark. Then the reaction solution was stirred under visible-light irradiation for several hours under the constant temperature at 25 °C. At given time intervals, 2 mL aliquots were sampled and filtered to remove the solid phase. The filtrates was tested by measuring the absorbance at 464 nm and 662 nm for MO and MB, respectively, by using UV–vis spectrophotometer (Shimadzu UV-2550 spectrometer) and the blank reaction was also carried out by the same procedure without adding any LDHs.

### 2.5. Regeneration of used Zn/Al–Ti/SB–LDHs

In the present work, we selected Zn/Al–Ti/SB–LDHs as the sample to determine the reutilization of Ti-based LDH materials as photo-catalysts for MO and MB removal from aqueous solutions, the used material was regenerated using a thermal recycle method like this: after completing equilibrium degradation experiments described in Section 2.4, the suspension was filtered and washed by water and ethanol (twice with each solvent) for complete cleaning of the catalyst, then the catalyst was dried at 65 °C for 12 h and redispersed in MO or MB solutions with known concentrations. This procedure was repeated three times and the amount of MO or MB after each dispersion–regeneration cycle was determined.

## 3. Results and discussion

### 3.1. Structural characteristics of Ti-based LDH

On the basis of ICP-AES and CHN analyses, the chemical composition of the samples was determined and the results are listed in Table 1. As shown in Table 1, the simplest molecular formula of these Ti-based LDHs is as follow: $Zn_{0.84}Ti_{0.16}(OH)_2(NO_3^-)_{0.35}{\cdot}0.39H_2O$, $[Zn_3Al(OH)_6NO_3](Ti/Schiff–base)_{0.34}{\cdot}0.58H_2O$ and $(CeO_2)_{0.23}(ZnO)_{4.76}(TiO_2)$, respectively. It is clear that the calculated values are in good agreement with the experiment data.

Fig. 1 shows the XRD patterns of Zn/Ti–LDHs (a), Zn/Al–LDHs (b), Zn/Al–Ti/SB–LDHs (c), $CeO_2$/ZnTi–LDH composite (d). The expected $d_{(003)}$ peaks were observed in the first three samples (a, b and c). And their XRD patterns also show the reflections of (0 0 6), (0 0 9), (0 1 2) and (1 1 0) which can be indexed to typical LDH materials

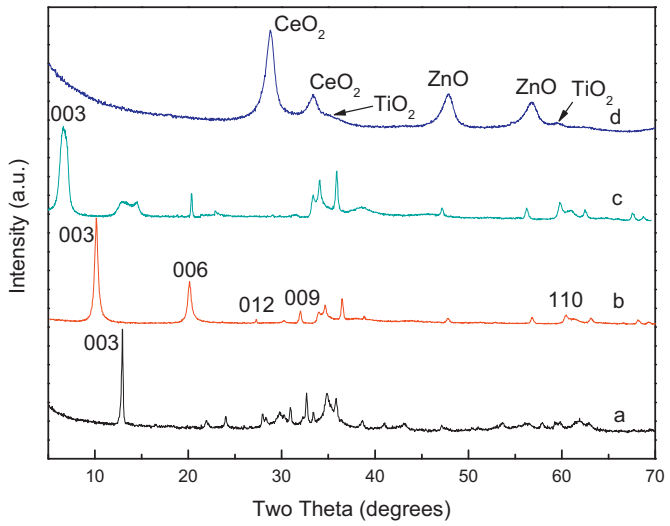


**Fig. 1.** The XRD patterns for Zn/Ti–LDHs (a), Zn/Al–LDHs (b), Zn/Al–Ti/SB–LDHs (c), $CeO_2$/ZnTi–LDH composite (d).

[22]. According to the XRD patterns of Zn/Ti–LDHs (Fig. 1a) and Zn/Al–LDHs (Fig. 1b), the interlayer distance ($d_{003}$) of Zn/Ti–LDHs and Zn/Al–LDHs are 0.66 nm ($2\theta = 13.2°$) and 0.76 nm ($2\theta = 11.7°$), respectively. This is consisted with the results reported by other authors [23,24]. While, for the Zn/Al–Ti/SB–LDHs (Fig. 1c), the interlayer distance ($d_{003}$) increases to 1.23 nm, and the thickness of the LDH layer is 0.48 nm [8], the gallery height of this sample after ion-exchange is 0.75 nm which can be calculated by the interlayer distance minus the thickness of the LDH layer. The increase in the basal distance confirms the intercalation of the Ti/SB complex. In addition, as expected, upon calcination, the XRD pattern of $CeO_2$/ZnTi–LDH composite (Fig. 1d) shows that layered structure of the original LDHs was completely destroyed and indicates only ZnO, $TiO_2$ and $CeO_2$ peaks [19,25], suggesting an almost total decomposition of the original LDHs and the formation of $CeO_2$/ZnTi–LDH composite.

For further investigation of the textural parameters of the Ti-based LDH materials, nitrogen sorption measurement was carried out. Fig. 2 shows the $N_2$ adsorption–desorption isotherm at 77 K and the corresponding pore size distribution curves for Zn/Ti–LDHs (A), Zn/Al–Ti/SB–LDHs (B), $CeO_2$/ZnTi–LDH composite (C). Both the isotherms for the first two samples are type II with a broad H3 type hysteresis loop ($P/P_0 < 0.4$) [26], indicating the presence of mesopores. Furthermore, any limiting adsorption at higher $P/P_0$ was not observed, indicating the existence of macropores [26]. This result can be confirmed by the corresponding wide distribution of pore size in Fig. 3A and B. In addition, though isotherms for both samples are quite similar, there are obvious differences in surface area, pore volume and pore size distribution. Zn/Al–Ti/SB–LDHs shows larger surface area (142 $m^2/g$), smaller pore volume (0.431 $cm^3/g$) and pore size (maximum at 16 nm and 50 nm) compared to Zn/Ti–LDHs. The isotherm for $CeO_2$/ZnTi–LDH composite is type IV (Fig. 2C), which is assigned to mesoporous structure, according to the IUPAC classification. Hysteresis loops are of type H3, which are commonly attributed to slit-shaped pores generated by the aggregation of plate-like particles [27]. The pore sizes are clearly defined, with three maximum at 4.5, 10 and 55 nm, and the mesopores (<50 nm) is contributing to the majority of the pore volume. The surface area of $CeO_2$/ZnTi–LDH composite is 198 $m^2/g$, which is the largest among the three materials.

Fig. 3 presents the infrared spectroscopy (IR) of as-synthesized samples. From the spectrum of Zn/Ti–LDHs (a) and Zn/Al–LDHs (b), according to the typical LDH structure [9], the FT-IR spectrum

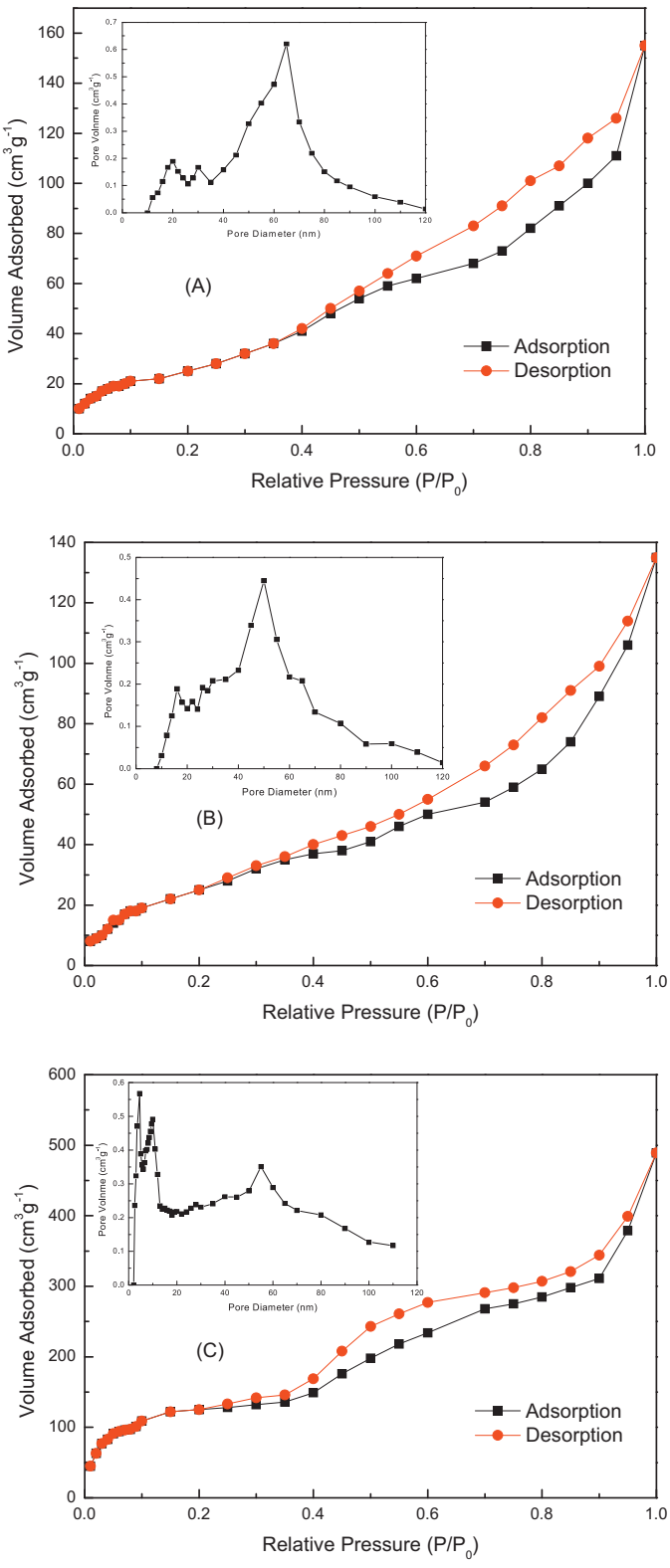


**Fig. 2.** $N_2$ sorption isotherms and pore size distribution of Zn/Ti–LDHs (A), Zn/Al–Ti/SB–LDHs (B), $CeO_2$/ZnTi–LDH composite (C).

of these three LDH samples can be roughly attributed as follows: (1) the broad absorption bands at 3440–3460 $cm^{-1}$ arises from the stretching mode of OH groups in the brucite-like layer and physisorbed water; (2) the band at 1610–1650 $cm^{-1}$ arises from H—O—H bending vibration; (3) the band at 1360–1380 $cm^{-1}$ arises from $NO_3^-$ stretching vibration, (4) the absorption bands below

**Table 1**
The chemical composition of Ti-based LDHs.

| Samples | Chemical formula | Ti% | $M^{II}/M^{III}/M^{V}$ |
|---|---|---|---|
| $Zn_5Ti–NO_3–LDHs$ | $Zn_{0.84}Ti_{0.16}(OH)_2(NO_3^-)_{0.35}\cdot 0.39H_2O$ | 6.1 | 5.25:1 |
| $Zn_3Al–NO_3–LDHs$ | $Zn_{0.74}Al_{0.26}(OH)_2(NO_3^-)_{0.32}\cdot 0.39H_2O$ | – | 2.85:1 |
| Ti/Schiff–base | $(C_{14}H_{10}NO_3Na)_{1.88}Ti$ | 8.9 | – |
| $Zn_3Al–Ti/SB–LDHs$ | $[Zn_3Al(OH)_6NO_3](Ti/Schiff–base)_{0.34}(CO_3^{2-})_{0.18}\cdot 0.58H_2O$ | 2.8 | 2.89:1:0.34 |
| $CeO_2/Zn_5Ti–LDH$ composite | $(CeO_2)_{0.23}(ZnO)_{4.76}(TiO_2)$ | 9.5 | 4.76:0.23 + 1 |

1000 $cm^{-1}$ are M—O vibration modes of LDHs, and the band at 400–500 $cm^{-1}$ is due to O—M—O vibration related to LDHs layers. In addition, for Ti/SB (c), the bands in the regions of 1610 and 1210 $cm^{-1}$ are due to C=N stretching of imine, and 1710 $cm^{-1}$ are due to C=O stretching of carboxylate group; after ion-exchange, Zn/Al–Ti/SB–LDHs (d) not only shows the similar structure with the original Zn/Al–LDH, but also appear the band at about 1625 $cm^{-1}$ and 1200 $cm^{-1}$ which is due to C=N stretching of imine, confirming the presence of Ti/Schiff–base anions inside the interlayer space. In addition, particularly, for Zn/Al–Ti/SB–LDHs (d), the weak bands observed at 1360 $cm^{-1}$ can be ascribed to the vibration of carbonate. Small amount of $CO_3^{2-}$ coexists between the layers is probably due to difficulty in completely avoiding contamination from air, which is in consistent with the chemical composition results (see Table 1). Finally, for $CeO_2$/ZnTi–LDH composite (e), as expected, the major bands almost vanish after the calcination process, revealing the removal of the anions from the LDH interlayer.

### 3.2. Photocatalytic properties of Ti-based LDH

The photo absorption properties of these Ti-based LDH materials detected by UV–vis spectrometer are shown in Fig. 4A. The absorbance of these three materials extends to the visible light region. In addition, according to the literature [28], the optical absorption of a crystalline semiconductor near the band edge can be calculated as follows (Eq. (1)):

$$\alpha h\upsilon = K(h\upsilon - E_g)^{n/2} \quad (1)$$

where $\alpha$, $h$, $\upsilon$, $K$, and $E_g$ are the absorption coefficient, Planck constant, light frequency, proportionality constant, and band gap, respectively. In addition, $n$ decides the characteristics of the transition in a semiconductor [29]: the $n$ value is 1, indicating the directly allowed optical transition. So, plot $(\alpha h\upsilon)^{2/n}$ vs. $h\upsilon$ and then the band gap $E_g$ can be obtained by extrapolating the linear region straight line to the $h\upsilon$ axis intercept as shown in Fig. 4B.

As shown in Fig. 4B, we can see that the band gap of Ti-based LDH materials were estimated to be 3.03 eV, 2.88 eV and 2.92 eV for Zn/Ti–LDHs, Zn/Al–Ti/SB–LDHs and $CeO_2$/ZnTi–LDH composite, respectively.

To demonstrate the feasibility of the application of Ti-based LDH materials in photocatalysis, the photodegradation of Methyl orange (MO) and Methylene blue (MB) was carried out with a reaction time ranging from 10 to 100 min, at 25 °C, pH 7.0, [MO] or [MB] = 50 mg/L and using 50 mg of LDH materials under visible-light irradiation. The results are presented in Fig. 5. We can see that the decomposition amounts of MO and MB increased rapidly in the initial 60 min and almost unchanged after 90 min (MO) and 100 min (MB), respectively, indicating reaching an equilibrium state. Photocatalyzed by these three LDH materials for 90 min (MO) or 100 min

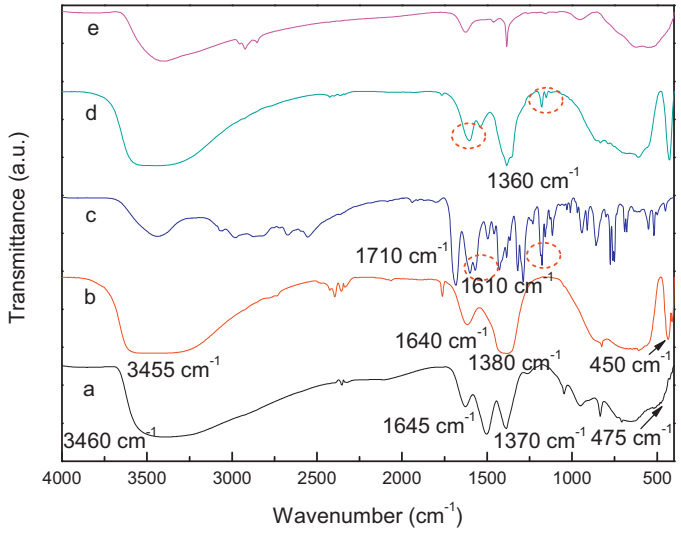


**Fig. 3.** The IR specturm for Zn/Ti–LDHs (a), Zn/Al–LDHs (b), Ti/SB (c), Zn/Al–Ti/SB–LDHs (d), $CeO_2$/ZnTi–LDH composite (e).

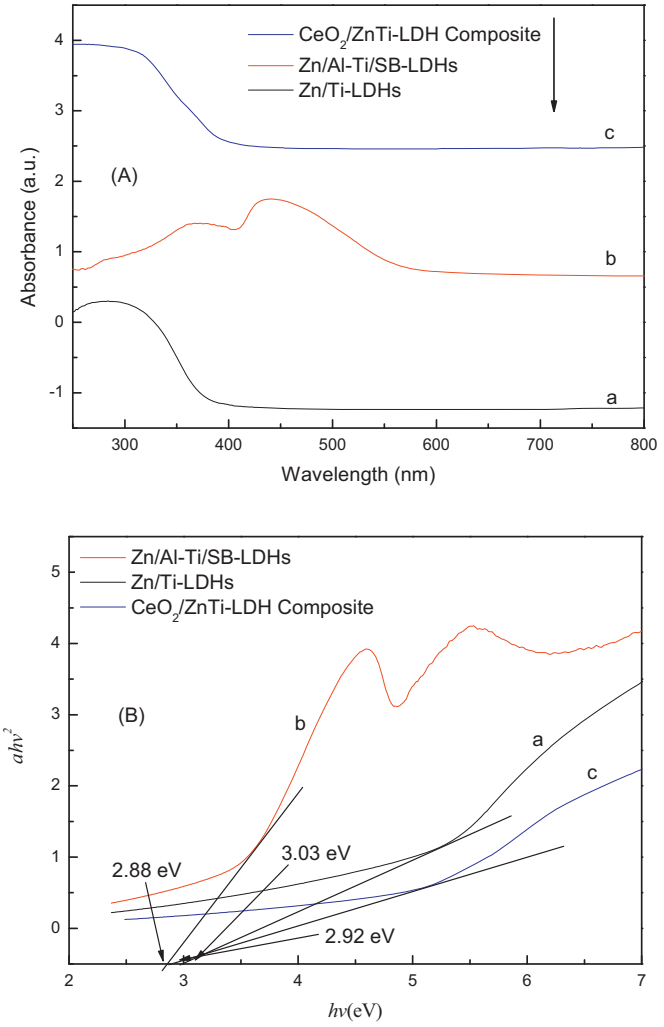


**Fig. 4.** The UV–vis curves (A) and plots of $(\alpha h\upsilon)^2$ *vs* $h\upsilon$ (B) for Zn/Ti–LDHs (a), Zn/Al–Ti/SB–LDHs (b), $CeO_2$/ZnTi–LDH composite (c).

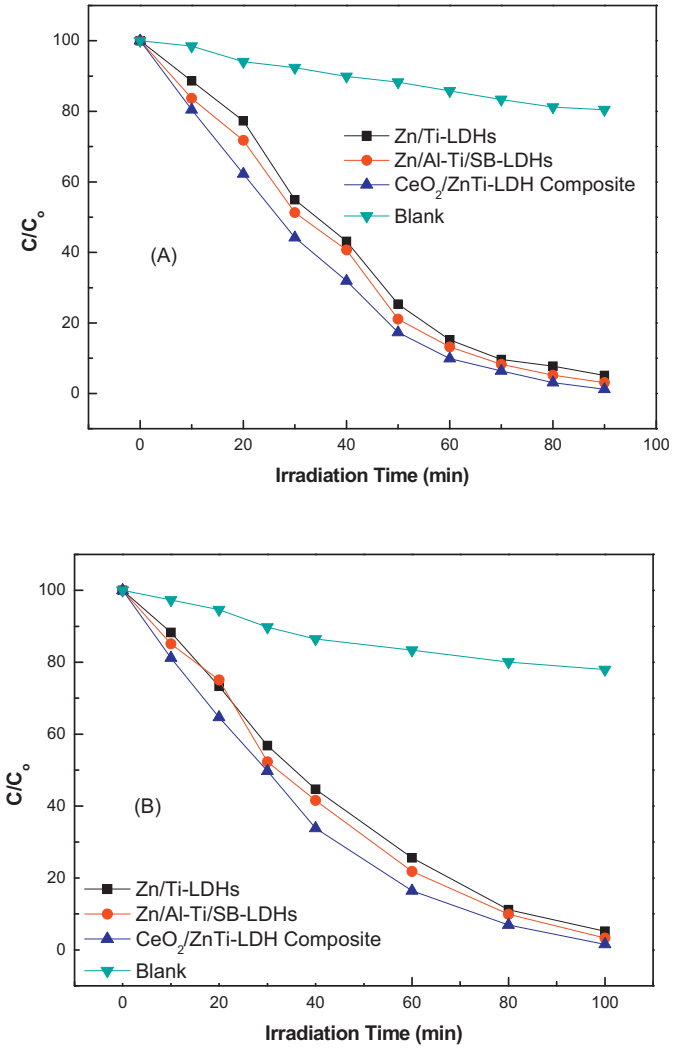


**Fig. 5.** Photodegradation of Methyl orange (A) and Methylene blue (B) monitored as the normalized concentration *vs* irradiation time under visible-light irradiation with the presence of different photocatalysts. Blank experiment means taking reaction system under vigorously stirred for 30 min to establish an adsorption/desorption equilibrium in dark before photocatalytic tests.

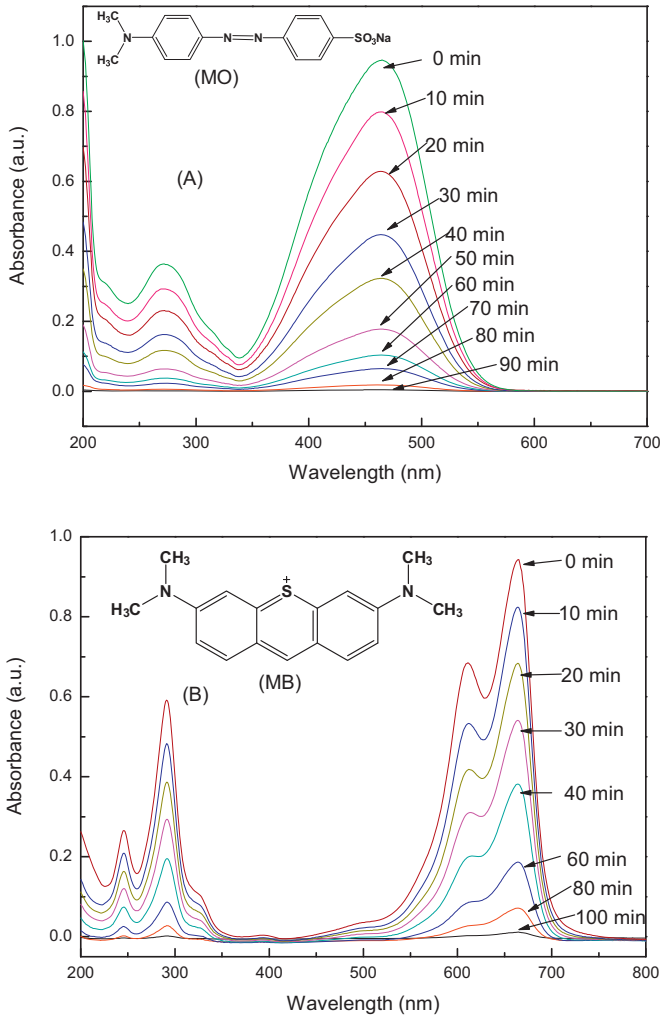


**Fig. 6.** Absorption changes of Methyl orange (A) and Methylene blue (B) during the photodegradation process over sample CeO$_2$/ZnTi–LDH composite under visible-light irradation.

(MB) more than 95% of the dyes degrade, and the decomposition performance is decreasing in the order of CeO$_2$/ZnTi–LDH materials > Zn/Al–Ti/SB–LDHs > Zn/Ti–LDHs both for MO and MB. It is obvious that all these Ti-based LDH materials exhibit high photocatalytic activity for MO and MB degradation under visible-light irradiation.

Particularly, it is observed that the band gap of Ti-based LDH materials decreases in the order of Zn/Ti–LDHs (3.03 eV) > CeO$_2$/ZnTi–LDHs (2.92 eV) > Zn/Al–Ti/SB–LDHs (2.88 eV); however, the degradation performance of MO and MB catalyzed by these three materials decreases in the order of CeO$_2$/ZnTi–LDHs > Zn/Al–Ti/SB–LDHs > Zn/Ti–LDHs. This phenomenon, which arises from the textural parameters of LDH materials, i.e. surface areas, pore volume and pore size (detected from BET and BJH method, see Table 2) is also very important for improving materials' photo activity besides the band gap. The high specific surface area is responsible for providing strong adsorption ability toward the target molecules and thus the generation of photoinduced electron–hole pairs of active sites are enhanced [30,31]. A wide distribution of macropores of LDH materials is favorable for the transportation and diffusion of species. In addition, other factors such as hierarchical structure and small crystallite size of LDH material may also attribute to its' high photocatalytic activity [32], which not only can facilitate the rapid transfer of photoelectrons from bulk to the surface, but also effectively inhibits the recombination between photoelectrons and holes.

Fig. 6 shows the relationship between absorbance and reaction time of photocatalytic degradation of Methyl orange and Methylene blue using CeO$_2$/ZnTi–LDH composite under visible light radiation. The strong absorption bands of Methyl orange (located at $\lambda = 338$ nm and $\lambda = 464$ nm) and Methylene blue (located at $\lambda = 291$ nm and $\lambda = 662$ nm) both decreased gradually upon the increasing of irradiation time, the absorbance of MO and MB solution were both about zero after irradiation for 90 min or 100 min with CeO$_2$/ZnTi–LDH catalyst.

The kinetics of Methyl orange and Methylene blue degradation catalyzed by Ti-based LDH materials were investigated based on the Langmuir–Hinshelwood model, which was commonly used to describe the kinetics of photocatalytic reactions of organic compounds in aqueous solutions [33]. It relates the degradation rate $r$ to the concentration of organic compound $C$, and is expressed as follows:

$$r = -\frac{dC}{dt} = \frac{k_r K_{ad} C}{1 + K_{ad} C} \quad (2)$$

**Table 2**
The band gap energy and textural properties of Ti-based LDH materials.

| Catalyst | Band gap energy (eV) | Surface area ($m^2/g$) | Pore volume ($cm^3/g$) | Pore size distribution (nm) |
|---|---|---|---|---|
| Zn/Ti–LDHs | 3.03 | 101 | 0.562 | 20, 30, 65 |
| Zn/Al–Ti/SB–LDHs | 2.88 | 142 | 0.431 | 16, 50 |
| $CeO_2$/ZnTi–LDH composite | 2.92 | 198 | 0.381 | 4.5, 10, 55 |

where $k_r$ is the intrinsic rate constant and $K_{ad}$ is the adsorption equilibrium constant. When the adsorption is relatively weak and the concentration of organic compounds is low, the factor $K_{ad}C$ is insignificant, therefore the equation can be simplified to the first-order kinetics with an apparent rate constant $K_{app}$, as Eq. (3) shows:

$$r = k_r K_{ad} C = K_{app} C \tag{3}$$

Setting Eq. (3) under initial conditions of photocatalytic procedure, ($t = 0$, $C = C_0$), Eq. (4) is obtained:

$$\ln \frac{C_0}{C} = K_{app} t \tag{4}$$

where $C_0$ and $C$ are the initial concentration of dye and the concentration at time $t$, respectively. The values of apparent rate constant ($K_{app}$) can be calculated from the gradient of the graph of $\ln(C_0/C)$ vs irradiation time by regression method.

Fig. 7 shows the photodegradation lineal plot of Methyl orange (A) and Methylene blue (B), which is adjusted well to a pseudo-first-order kinetic behavior (linearly dependent coefficients all over 0.96, see Table 3). In addition, the apparent rate constant $K_{app}$ and dyes half-life $t_{1/2}$ of all these materials are also given in Table 3. Basically, over half of Methyl orange and Methylene blue degrade photocatalyzed by all these LDH materials after a 22 min reaction, the values of dyes half-life $t_{1/2}$ were decreasing in the order of $CeO_2$/ZnTi–LDH composite > Zn/Al–Ti/SB–LDHs > Zn/Ti–LDHs for both MO and MB decomposition. Particularly, the rate constant was calculated to be 0.0479 $min^{-1}$ ($t_{1/2}$ = 14.5 min) and 0.0429 $min^{-1}$ ($t_{1/2}$ = 16.2 min) for MO and MB, respectively, with $CeO_2$/ZnTi–LDH composite as the photocatalyst, that is to say, the decomposition of Methyl orange and Methylene blue using $CeO_2$/ZnTi–LDH composite reached 50% only after 14.5 min and 16.2 min of reaction, respectively, which is considerably efficient.

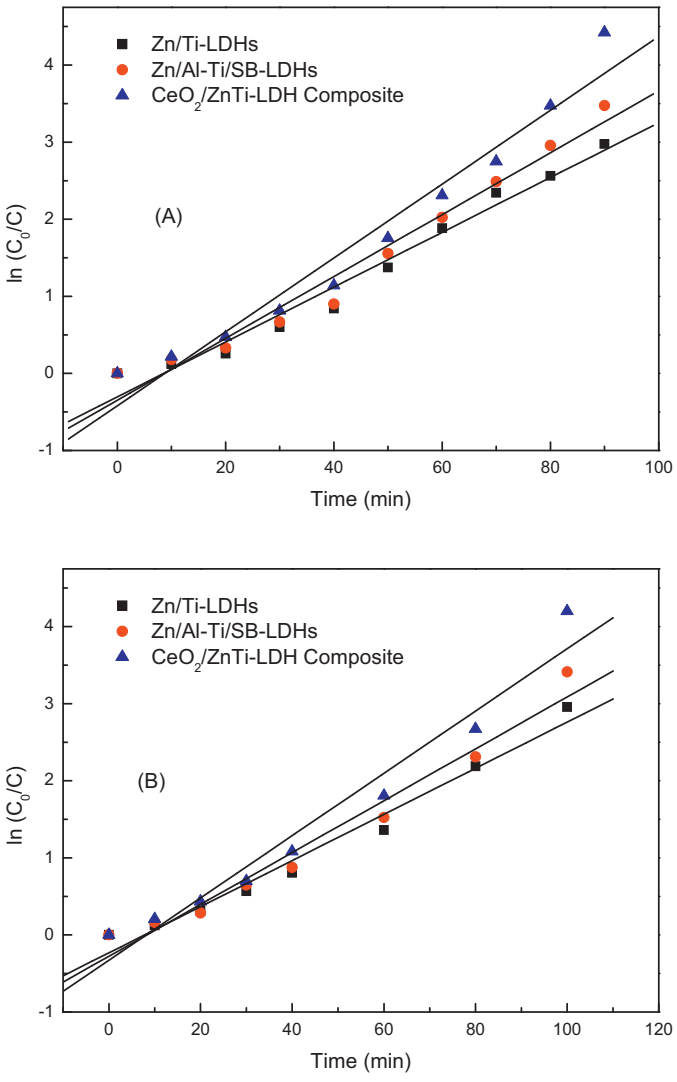


**Fig. 7.** Pseudo first-order kinetics degradation for Methyl orange (A) and Methylene blue (B), by Langmuir–Hinshelwood model.

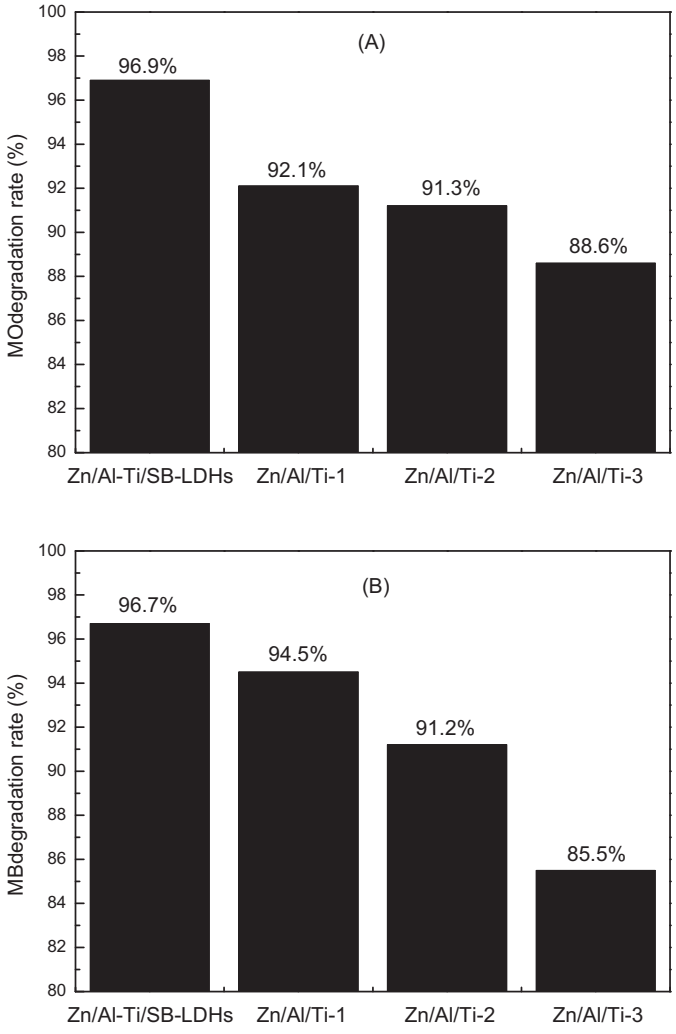


**Fig. 8.** Comparison of Methyl orange (A) and Methylene blue (B) decomposition between original Zn/Al–Ti/SB–LDHs and thermally regenerated materials from used LDHs. Thereinto, Zn/Al/Ti-1, Zn/Al/Ti-2 and Zn/Al/Ti-3 are the products after the first-, second- and third-cycle thermal regenerations of Zn/Al–Ti/SB–LDHs, respectively.

**Table 3**
Pseudo first order kinetic parameters for dyes photodegradation.

| Sample | MO | | | MB | | |
|---|---|---|---|---|---|---|
| | $K_{app}$ ($min^{-1}$) | $t_{1/2}$ (min) | $r^2$ | $K_{app}$ ($min^{-1}$) | $t_{1/2}$ (min) | $r^2$ |
| ZnTi–$NO_3$–LDHs | 0.0356 | 19.5 | 0.9750 | 0.0317 | 21.9 | 0.9858 |
| ZnAl–Ti/SB–LDHs | 0.0401 | 17.3 | 0.9721 | 0.0357 | 19.4 | 0.9775 |
| $CeO_2$/ZnTi–LDH composite | 0.0479 | 14.5 | 0.9615 | 0.0429 | 16.2 | 0.9664 |

With the aim of determining the reutilization of Ti-based LDH materials as efficient photocatalysts for the removal of Methyl orange and Methylene blue, thermal regeneration tests were carried out and the results are shown in Fig. 8 (Zn/Al–Ti/SB–LDHs was chose as a sample). It shows that the progressive reduction after three cycles regeneration is very small, the decomposition of Methyl orange decreases by only 4.8%, 5.6%, and 8.3% (from 96.9% to 92.1%, 91.3% and 88.6% for first-, second-, and third-cycle), respectively, the decomposition of Methylene blue decreases by only 2.2%, 5.7%, and 11.2% (from 96.7% to 94.5%, 91.2% and 85.5%), respectively, compared with the original Zn/Al–Ti/SB–LDHs. This indicates that the Zn/Al–Ti/SB–LDHs is stable enough as photocatalyst, and the thermal regeneration for re-use of Zn/Al–Ti/SB–LDHs after MO or MB photodecomposition was feasible for at least three cycles.

### 3.3. Mechanism and discussion on visible light photocatalytical reaction using Ti-based LDH

According to the experimental results, a possible mechanism and the intermediates are proposed and discussed as follow (Methyl orange was chose as a sample to depict).

The first stage, when a Ti-based LDH material molecule absorb a photon with energy equal to or higher than its band gap, the excited electrons of LDH materials are promoted from the valence band to the conduction band yielding holes ($h^+$) and photon generated electrons ($e^-$) (see Eq. (5)). And then, this electron–hole pair ($e^-/h^+$) reacts with water and dissolved oxygen to produce hydroxyl radicals ($OH^\bullet$) (see Eqs. (6)–(10)).

$$\text{Ti-based-LDHs} \xrightarrow{h\upsilon} h^+ + e^- \quad (5)$$

$$h^+ + H_2O \rightarrow OH^\bullet + H^+ \quad (6)$$

$$e^- + O_2 \rightarrow O_2^{\bullet -} \quad (7)$$

$$O_2^- + H^+ \rightarrow HOO^\bullet \quad (8)$$

$$e^- + HOO^\bullet + H^+ \rightarrow H_2O_2 \quad (9)$$

$$H_2O_2 + e^- \rightarrow OH^\bullet + OH^- \quad (10)$$

Photon generated electrons ($e^-$) are reducing oxidizing agents, while the hydroxyl radicals ($OH^\bullet$) are strong oxidizing agents for organic pollutants. Thus, the second stage, one side, hydroxyl radicals are electrophilic reagents, the possible major reactions between $OH^\bullet$ and organic compounds are additive reaction, electron transfer reaction, and hydrogen abstraction reaction. The possible reaction mechanism between $OH^\bullet$ and methyl orange is given as follow (Eq. (11)):

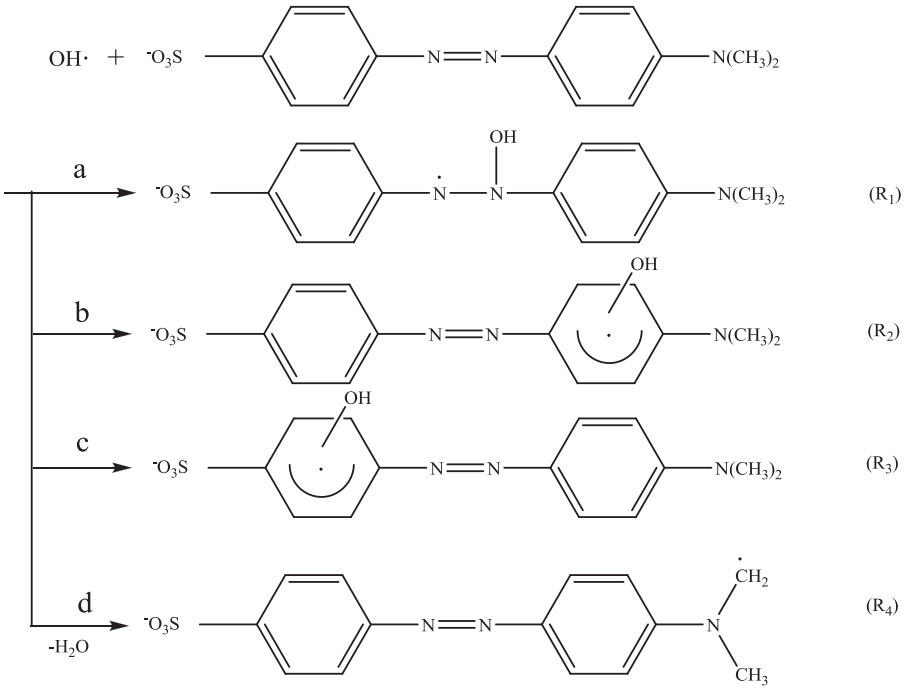


(11)

Because of the conjugation effect of methyl orange, the electron donating effect of methylamino and also the electrophilic of sulfuric acid root, the electron density of the azo and methylamino group is very high, but the benzene ring electron density is very low at the same time, therefore the contribution from c and d is very small. We also predict that the —OH is attached to the *o*-, *p*-positions of the methylamino-group. Therefore, with the breaking of N=N, $R_1$ or

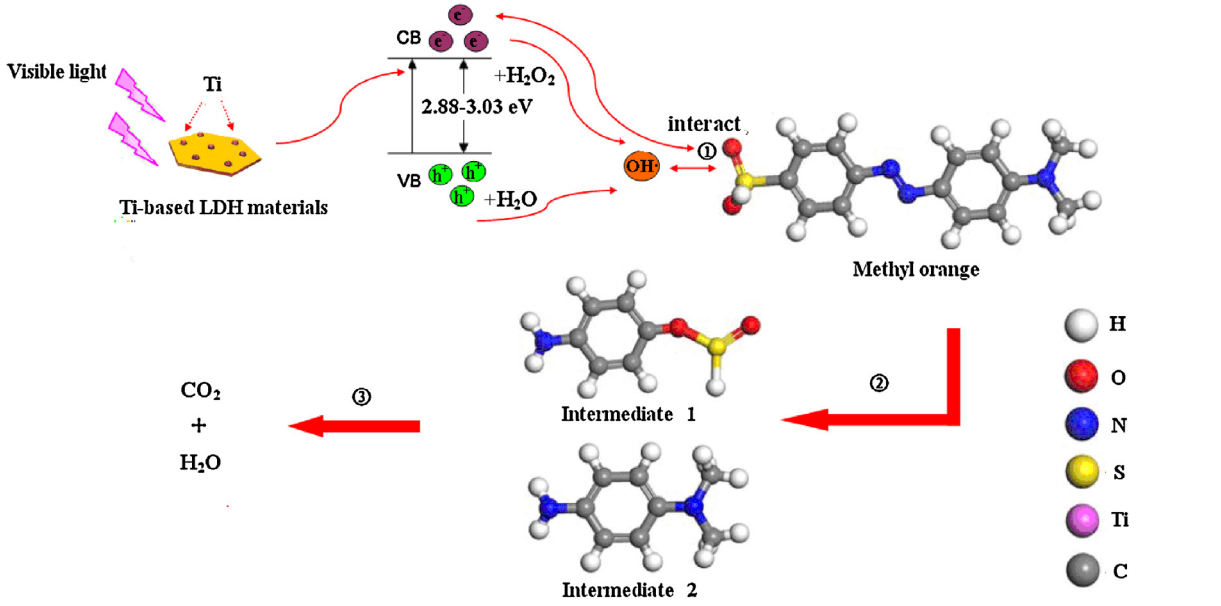


**Fig. 9.** The possible mechanism for photocatalytic degradation of Methyl orange over Ti-based LDH materials.

$R_2$ may finally further decompose to *p*-amino-*N*,*N*-dimethylaniline and *p*-aminobenzene sulfonic acid (see Eq. (12)).

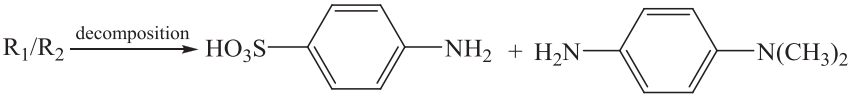


(12)

On the other hand, hydrated electron is a typical nucleophilic reagent, it attacks the azo connected benzene ring which has a very low electron density, and produces radical anion (MO·⁻), MO·⁻ is very unstable and quickly protonated into MOH·, also, MOH· could be further reduced and protonated, and bring in the break of N=N, and finally the formation of *p*-amino-*N*,*N*-dimethylaniline and *p*-aminobenzene sulfonic acid (see Eq. (13)).

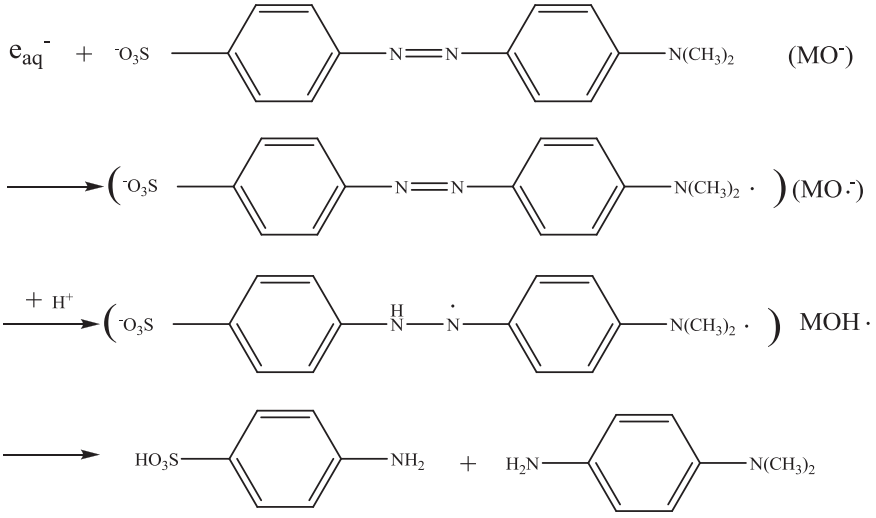


(13)

Finally, the intermediates of *p*-amino-*N*,*N*-dimethylaniline and *p*-aminobenzene sulfonic acid could be further decomposed into inorganic micromolecules, like carbon dioxide and water. Fig. 9 is the schematic illustration of Methyl orange photodegradation catalyzed by Ti-based LDH materials.

## 4. Conclusions

The good crystal structure of Zn/Ti–$NO_3$–LDHs with Ti element on LDH sheet, Zn/Al–Ti/Schiff–base–LDHs with Ti element in LDH

interlayer and $CeO_2$/ZnTi–LDH composite containing $TiO_2$ can be successfully synthesized by coprecipitation, ion-exchange, and calcination method, respectively. And all these Ti-based LDH materials displayed high photocatalytic activity under visible-light irradiation for Methyl orange and Methylene blue dregradation. The values of decomposition efficiency of Methyl orange and Methylene blue by these three materials are all over 95% after 100 min of reaction, the values decreasing in the order of $CeO_2$/ZnTi–LDH composite > Zn/Al–Ti/Schiff–base–LDHs > Zn/Ti–$NO_3$–LDHs. The $CeO_2$/ZnTi–LDH composite shows the highest photocatalytic activity among the four samples, under the experimental condition of 298 K, pH 7.0, 50 mg/L for Methyl orange or Methylene blue solution and 50 mg for LDH material under irradiation with visible-light. In addition, the degradation kinetics can be successfully fitted to pseudo-first-order kinetic model. Zn/Al–Ti/Schiff–base–LDHs are stable and able to be reused at least three times. Hence, this work demonstrates that the synthesized Ti-based LDH materials with rather high photocatalytic activity in the visible-light region, could be potentially applied in the field of azo dyes removal.

## References


[1] D.Q. Zhang, G.S. Li, H.X. Li, Y.F. Lu, Chem.-Asian J. 8 (2013) 26–40.
[2] S. Linic, P. Christopher, D.B. Ingram, Nat. Mater. 10 (2011) 911–921.
[3] M.A. Lazar, W.A. Daoud, RSC Adv. 3 (2013) 4130–4140.
[4] K. Takanabe, K. Domen, Chemcatchem 4 (2012) 1485–1497.
[5] M. Sanchez, M.J. Rivero, I. Ortiz, Appl. Catal. B 101 (2011) 515–521.
[6] L. Teruel, Y. Bouizi, P. Atienzar, V. Fornes, H. Garcia, Energy Environ. Sci. 3 (2010) 154–159.
[7] Z.M. Ni, S.J. Xia, L.G. Wang, F.F. Xing, G.X. Pan, J. Colloid Interface Sci. 316 (2007) 284–291.
[8] Q. Wang, D. O'Hare, Chem. Rev. 12 (2012) 4124–4155.
[9] M.Q. Zhao, Q. Zhang, J.Q. Huang, F. Wei, Adv. Funct. Mater. 22 (2012) 675–694.
[10] L. Ye, H. You, J. Yao, H.L. Su, Desalination 298 (2012) 1–12.
[11] L. Tian, Y.F. Zhao, S. He, M. Wei, X. Duan, Chem. Eng. J. 184 (2012) 261–267.
[12] K. Dutta, S. Das, A. Pramanik, J. Colloid Interface Sci. 366 (2012) 28–36.
[13] E. Dvininov, M. Ignat, P. Barvinschi, M.A. Smithers, E. Popovici, J. Hazard. Mater. 177 (2010) 150–158.
[14] Y.F. Zhao, M. Wei, J. Lu, Z.L. Wang, X. Duan, ACS Nano 3 (2009) 4009–4016.
[15] K. Teramura, S. Iguchi, Y. Mizuno, T. Shishido, T. Tanaka, Angew. Chem. Int. Ed. 51 (2012) 8008–8011.
[16] C.G. Silva, Y. Bouizi, V. Forne's, H. Garcı'a, J. Am. Chem. Soc. 131 (2009) 13833.
[17] X. Shu, J. He, D. Chen, J. Phys. Chem. C 112 (2008) 4151–4158.
[18] Z.J. Huang, P.X. Wu, Y.H. Lu, X.R. Wang, N.W. Zhu, Z. Dang, J. Hazard. Mater. 246 (2013) 70–78.
[19] J.S. Valente, F. Tzompantzi, J. Prince, Appl. Catal. B 102 (2011) 276–285.
[20] R.J. Lu, X. Xu, J.P. Chang, Y. Zhu, S.L. Xu, F.Z. Zhang, Appl. Catal. B 111–112 (2012) 389–396.
[21] L.F. Chepik, E.P. Troshina, T.S. Mashcenko, D.P. Romanov, A.I. Maksimov, O.F. Lutskaya, Russ. J. Appl. Chem. 74 (2001) 1617–1620.
[22] Z.P. Xu, H.C. Zeng, J. Phys. Chem. B 105 (2001) 1743–1749.
[23] Z.L. Wang, Z.H. Kang, E.B. Wang, Z.M. Su, L. Xu, Inorg. Chem. 45 (2006) 4364–4371.
[24] K.M. Parida, L. Mohapatra, Chem. Eng. J. 179 (2012) 131–139.
[25] Y.W. Zhang, R. Si, C.S. Liao, C.H. Yan, C.X. Xiao, Y. Kou, J. Phys. Chem. B 107 (2003) 10159–10167.
[26] J. Yu, S. Liu, H. Yu, J. Catal. 249 (2007) 59–66.
[27] K.S.W. Sing, D.H. Everett, R.A.W. Haul, L. Moscou, R.A. Pierotti, J. Rouquerol, T. Siemieniewska, Pure Appl. Chem. 57 (1985) 603–619.
[28] M. Alvarez, T. López, J.A. Odriozola, M.A. Centeno, M.I. Domínguez, M. Montes, P. Quintana, D.H. Aguilar, R.D. González, Appl. Catal. B 73 (2007) 34–41.
[29] J.S. Valente, F. Tzompantzi, J. Prince, J.G.H. Cortez, R. Gomez, Appl. Catal. B 90 (2009) 330–338.
[30] M.A. Carreon, S.Y. Choi, M. Mamak, N. Chopra, G.A. Ozin, J. Mater. Chem. 17 (2007) 82–89.
[31] S.Y. Chae, M.K. Park, S.K. Lee, T.Y. Kim, S.K. Kim, W.I. Lee, Chem. Mater. 15 (2003) 3326–3331.
[32] M.F. Shao, J.B. Han, M. Wei, D.G. Evans, X. Duan, Chem. Eng. J. 168 (2011) 519–524.
[33] H. Fu, C. Pan, W. Yao, Y. Zhu, J. Phys. Chem. B 109 (2005) 22432–22439.